Cell Reports, Volume *43*

Supplemental information

Recruitment of BAG2 to DNAJ-PKAc scaffolds promotes cell survival and resistance to drug-induced apoptosis in fibrolamellar carcinoma

Sophia M. Lauer, Mitchell H. Omar, Martin G. Golkowski, Heidi L. Kenerson, Kyung-Soon Lee, Bryan C. Pascual, Huat C. Lim, Katherine Forbush, F. Donelson Smith, John D. Gordan, Shao-En Ong, Raymond S. Yeung, and John D. Scott

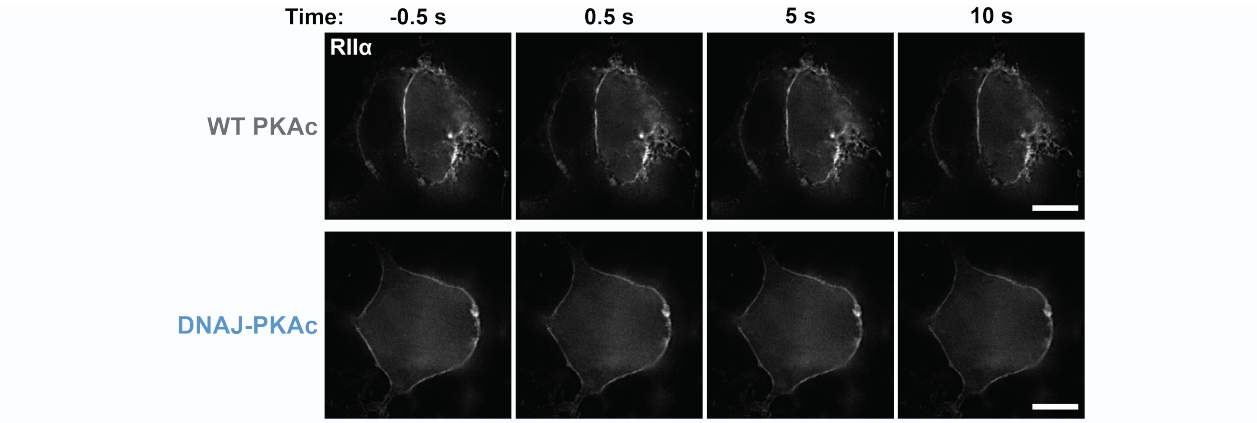

Figure S1. RIIα remains colocalized with membrane-associated AKAP79, related to Figure 2

Photoactivation timecourses showing RIIα-iRFP localization in AML12 hepatocytes expressing AKAP79-GFP, RIIα-iRFP, and either WT PKAc (top row) or DNAJ-PKAc (bottom row) tagged with photoactivatable mCherry. Scale bar = 10 μm. Data represents 3 experimental replicates.

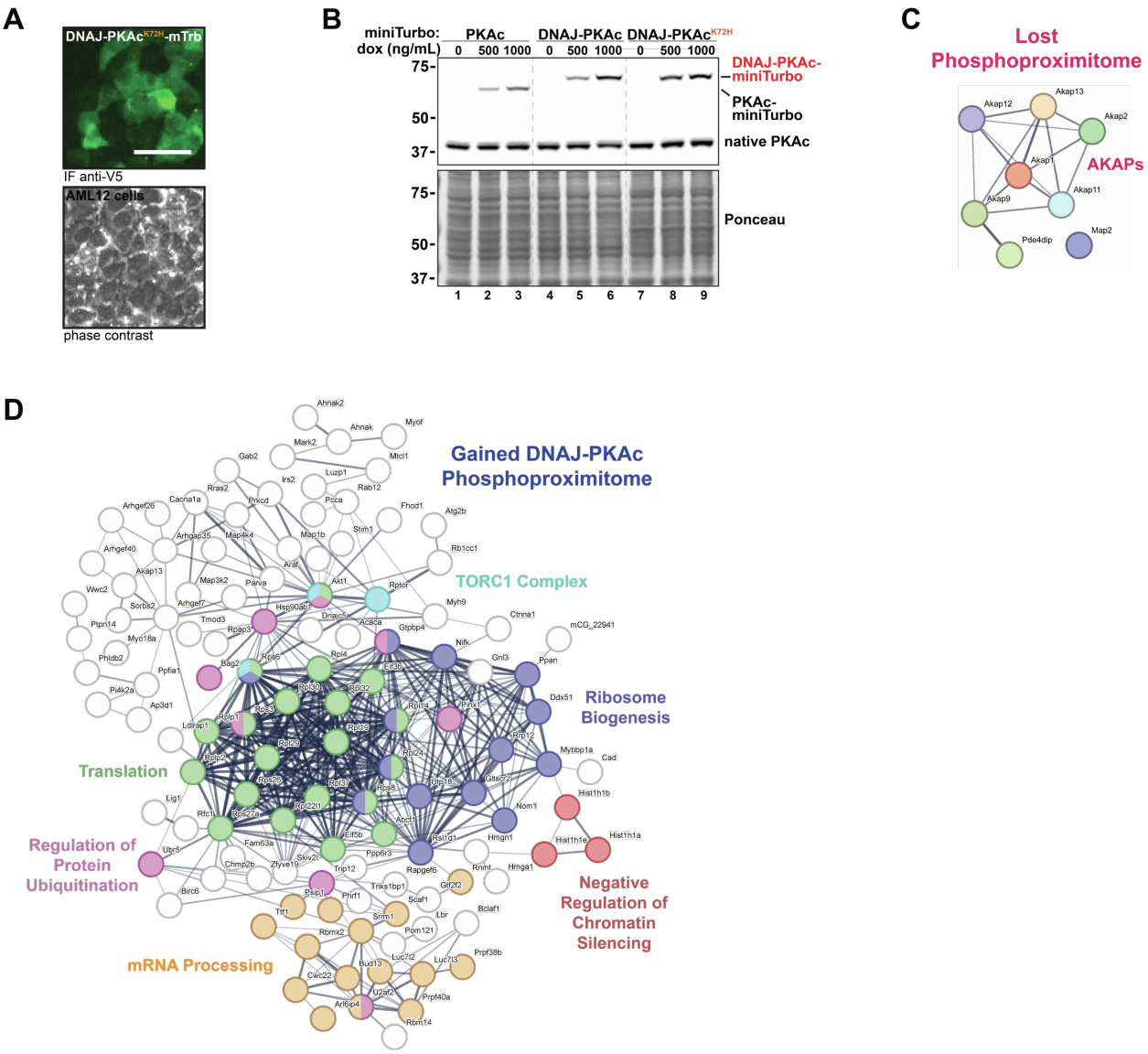

Figure S2. Proximity phosphoproteomic analysis reveals altered phosphorylation of biological process components in the presence of DNAJ-PKAc, related to Figure 3

A) Immunofluorescence imaging of AML12 hepatocytes demonstrating inducible expression of DNAJ-PKAc^{K72H}-mTrb (green, top) with corresponding phase contrast (bottom). Scale bar = 50 μm.

B) Immunoblot of cell lysate from AML12 stable lines demonstrating doxycycline-inducible expression of miniTurbo-tagged PKAc variants (top bands) and native PKAc (bottom bands). Dashed line removes lanes from a separate experiment.

C) STRING network depiction of selected phosphoproteins with lesser enrichment in DNAJ-PKAc versus WT PKAc.

D) STRING network depiction of selected phosphoproteins with greater enrichment in DNAJ-PKAc versus WT PKAc. Node color corresponds with similarly colored annotation.

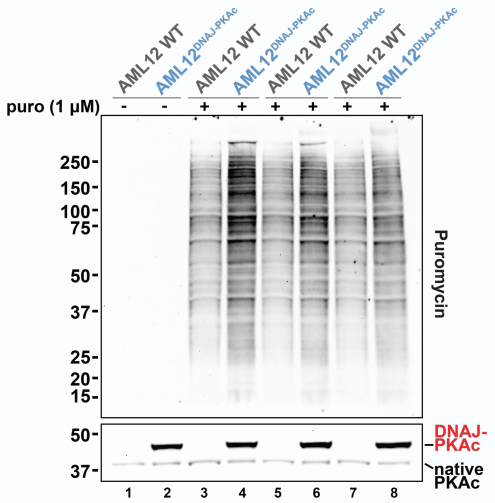

Figure S3. Cells expressing DNAJ-PKAc exhibit enhanced translation, related to Figure 4
Full immunoblot showing three biological replicates of cell lysates from WT AML12 and AML12$^{DNAJ\text{-}PKAc}$ treated with either vehicle or puromycin (1 μM). Puromycin conditions in top panel show newly synthesized, puromycin-labeled proteins. PKAc in bottom panel shows expression of DNAJ-PKAc (top band) over native PKAc (bottom band).

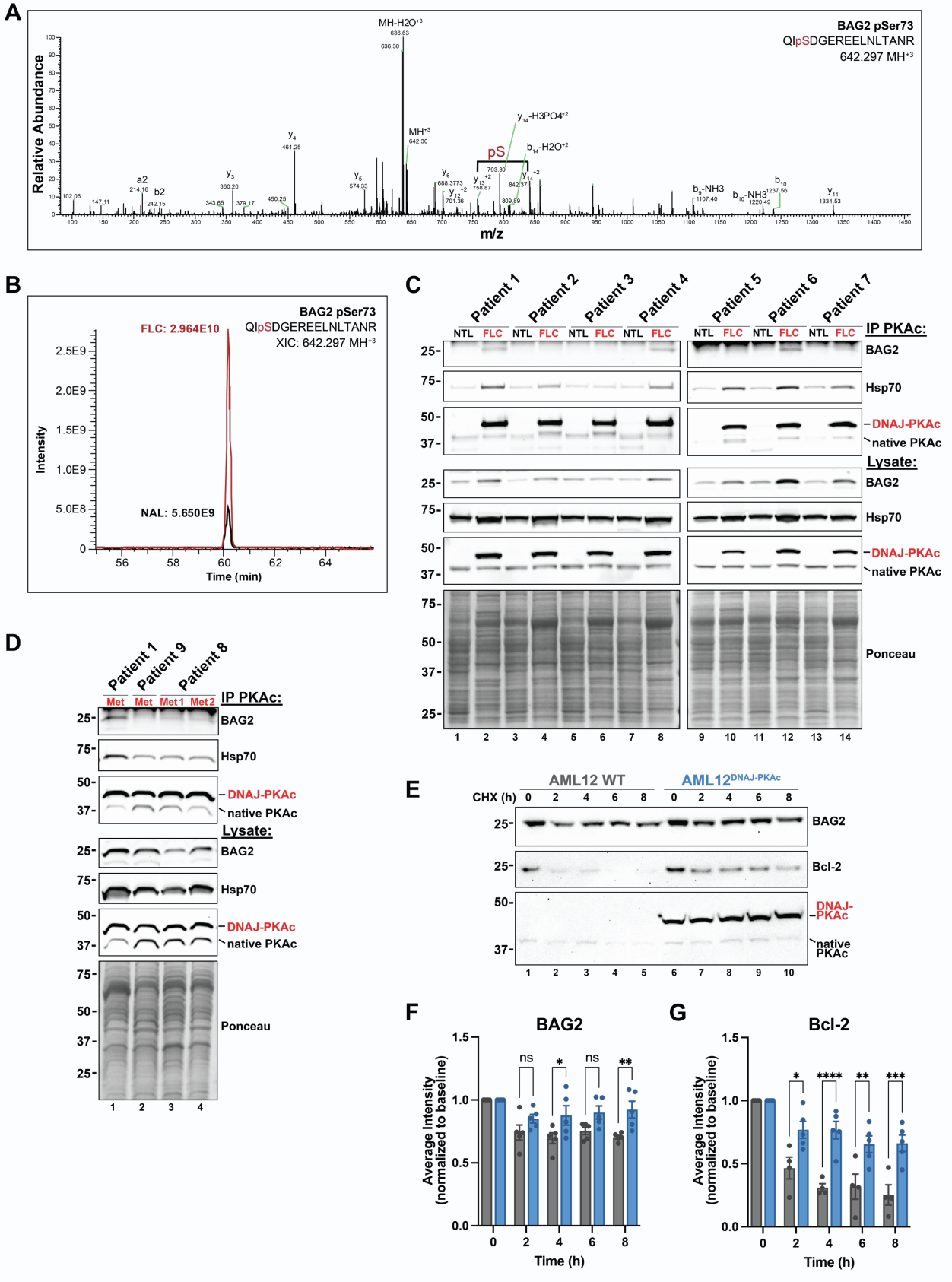
A
BAG2 pSer73
QIpSDGEREELNLTANR
642.297 MH+3
Relative Abundance
m/z
MH-H2O+3
MH+3
pS
y4
y3
y5
y6
a2
b2
y14-H3PO4+2
b14-H2O+2
B
BAG2 pSer73
QIpSDGEREELNLTANR
XIC: 642.297 MH+3
FLC: 2.964E10
NAL: 5.650E9
Intensity
Time (min)
C
Patient 1
Patient 2
Patient 3
Patient 4
Patient 5
Patient 6
Patient 7
NTL
FLC
IP PKAc:
BAG2
Hsp70
DNAJ-PKAc
native PKAc
Lysate:
Ponceau
D
Patient 1
Patient 9
Patient 8
Met
Met1
Met2
IP PKAc:
BAG2
Hsp70
DNAJ-PKAc
native PKAc
Lysate:
Ponceau
E
AML12 WT
AML12DNAJ-PKAc
CHX (h)
BAG2
Bcl-2
DNAJ-PKAc
native PKAc
F
BAG2
Average Intensity (normalized to baseline)
Time (h)
ns
*
**
G
Bcl-2
Average Intensity (normalized to baseline)
Time (h)
*
****
**
***

Figure S4. BAG2 phosphorylation and stability is enhanced in the presence of DNAJ-PKAc, related to Figure 5

A) MS2 spectrum of BAG2 pSer73 phosphopeptide. An Orbitrap-HCD MS2 spectrum of BAG2 phosphopeptide QIpSDGEREELNLTANR (+3) is labeled with fragment ions localizing the phosphoserine residue.

B) Extracted ion chromatograms of BAG2 pSer73 phosphopeptide. The ion chromatograms for the triply charged BAG2 phosphopeptide were extracted from LC-MS runs from FLC (red) and normal adjacent liver (NAL; black). Peak areas were determined using the ICIS peak detection algorithm in FreeStyle 1.8SP2 (Thermo Fisher). The data shows that BAG2 pSer73 phosphopeptide is up 5.2 fold in FLC over normal.

C) Immunoprecipitation with antibody against PKAc from paired normal adjacent liver (NTL) and FLC tumor (FLC) tissue lysates from 7 patients.

D) Immunoprecipitation with antibody against PKAc from tumor tissue lysates of four metastatic (Met) recurrences across 3 patients.

E) Immunoblot detection of BAG2 and Bcl-2 following cycloheximide (CHX) treatment. AML12 WT (lanes 1-5) and AML12$^{DNAJ\text{-}PKAc}$ (lanes 6-10) cell lysates were harvested at 0, 2, 4, 6, and 8 hours post-CHX treatment. Data represents 5 experimental replicates.

F) Quantification of (E) measuring amount of BAG2 protein remaining following CHX treatment at each time point in WT AML12 cells (grey) and AML12$^{DNAJ\text{-}PKAc}$ cells (blue). Data represents 4 experimental replicates. Mean ± SEM. **p≤0.01, *p≤0.05.

G) Quantification of (E) measuring amount of Bcl-2 protein remaining following CHX treatment at each time point in WT AML12 cells (grey) and AML12$^{DNAJ\text{-}PKAc}$ cells (blue). Data represents 5 experimental replicates. Mean ± SEM. ****p≤0.0001, ***p≤0.001, **p≤0.01, *p≤0.05.

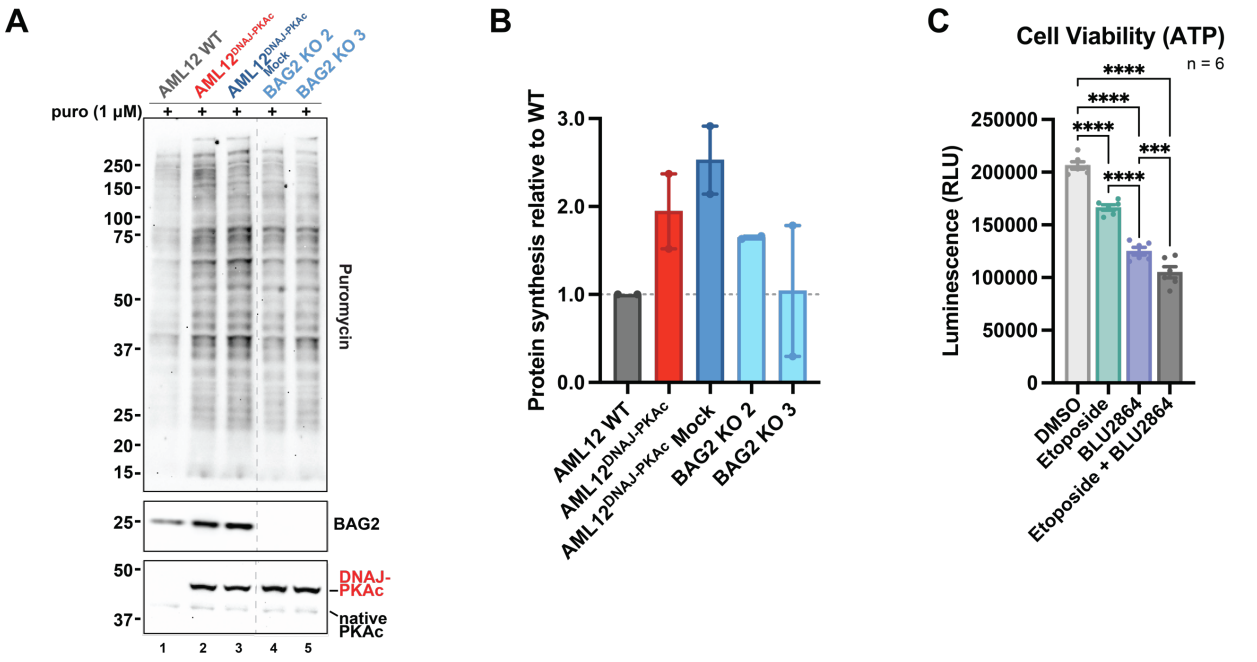

Figure S5. BAG2 KO and inhibition of kinase activity in cells expressing DNAJ-PKAc reduce protein synthesis and viability, respectively, related to Figure 6

A) Immunoblot of cell lysates from WT AML12, AML12$^{DNAJ\text{-}PKAc}$, AML12$^{DNAJ\text{-}PKAc}$ Mock control cell line, and two AML12$^{DNAJ\text{-}PKAc}$ BAG2 KO clones treated with puromycin (1 μM). Puromycin conditions in top panel show newly synthesized, puromycin-labeled proteins. Middle panel shows BAG2 expression in each cell line. PKAc in bottom panel shows expression of DNAJ-PKAc (top band) over native PKAc (bottom band). Dashed line removes lanes from a separate experiment.

B) Quantification of (A) measuring protein synthesis in WT AML12, AML12$^{DNAJ\text{-}PKAc}$, AML12$^{DNAJ\text{-}PKAc}$ Mock control cell line, and two AML12$^{DNAJ\text{-}PKAc}$ BAG2 KO clones. Data represents 2 biological replicates. Mean ± SEM.

C) Quantification of CellTiter-Glo luminescent assay showing cell viability of FLX1 cells following treatment with either vehicle, etoposide (50 μM), BLU2864 (5 μM), or etoposide (50 μM) and BLU2864 (5 μM) for 120 hours. Data represents 6 technical replicates. Mean ± SEM. ****p≤0.0001, ***p≤0.001.